Large area roll-to-roll printed semiconducting carbon nanotube thin films for flexible carbon-based electronics

Jiaqi Li[1,2,3], Min Li[2,3], Zhaofeng Chen[3], Shuangshuang Shao[2,3], Weibing Gu[2,3], Ying Gu[1,2,3], Yuxiao Fang[2,3]*, Jianwen Zhao[2,3]*

[1]Institute of Nano Science and Technology, University of Science and Technology of China, No. 166 Ren Ai Road, Suzhou Industrial Park, Suzhou, Jiangsu Province, 215123, PR China

[2]School of Nano-Tech and Nano-Bionics, University of Science and Technology of China, No. 398 Ruoshui Road, Suzhou Industrial Park, Suzhou, Jiangsu Province, 215123, PR China

[3] Division of Nanodevices and Related Nanomaterials, Suzhou Institute of Nano-Tech and Nano-Bionics, Chinese Academy of Sciences, No. 398 Ruoshui Road, Suzhou Industrial Park, Suzhou, Jiangsu Province, 215123, PR China

* Corresponding authors.

Email: J.W. Zhao (jwzhao2011@sinano.ac.cn);

　　　　Y.X. Fang (yxfang2021@sinano.ac.cn).

Abstract

A universal roll-to-roll (R2R) printing approach was developed to construct large area (8 cm × 14 cm) semiconducting single-walled carbon nanotubes (sc-SWCNT) thin films on flexible substrates (such as polyethylene terephthalate (PET), paper, and Al foils) with a printing speed of 8 m min^{-1} using highly concentrated sc-SWCNT inks and crosslinked poly-4-vinylphenol (c-PVP) as the adhesion layer. Bottom-gated and top-gated flexible printed p-type TFTs based on R2R printed sc-SWCNT thin films exhibited good electrical properties with carrier mobility of ~11.9 cm^2 V^{-1} s^{-1}, I_{on}/I_{off} ratios of ~10^6, small hysteresis, and subthreshold swing (SS) of 70-80 mV dec^{-1} at low gate operating voltages (±1 V), and excellent mechanical flexibility. Furthermore, the flexible printed complementary metal oxide semiconductor (CMOS)

inverters demonstrated rail-to-rail voltage output characteristics under the operating voltage down to V_{DD} = -0.2 V, voltage gain of 10.8 at V_{DD} = -0.8 V, and power consumption down to 0.056 nW at V_{DD} = -0.2 V. To the best of our knowledge, the electrical properties of printed SWCNT TFTs (such as I_{on}/I_{off} ratio, mobility, operating voltage, and mechanical flexibility) and printed CMOS inverters based on R2R printed sc-SWCNTactive layer in this work are more excellent compared to R2R printed SWCNT TFTs reported in the literature. Consequently, the universal R2R printing method reported in this work could promote the development of fully printed low-cost, large-area, high-output, and flexible carbon-based electronics.

Keywords: Roll-to-roll (R2R) gravure printing, Single-walled carbon nanotubes, Thin film transistors, Flexible CMOS inverter

1. Introduction

In recent years, printed electronics[1-3] and their applications have been intensively studied and achieved tremendous development,[1, 4] owing to new materials and the improvement of printing technology.[5-8] The potential of this additive manufacturing technique for low-cost mass production, rapid prototyping of small series, and low-temperature fabrication on flexible substrates[9, 10] renders it an attractive alternative to conventional fabrication methods for electronics.[11] It is known that the properties of channel materials determine the electrical properties of printed thin film transistors (TFTs).[12] Solution-processable semiconductor materials in the forms of organic compounds,[3, 13-16] graphene,[17-22] carbon nanotubes, and oxides[23, 24] have been developed to be compatible with current printing techniques.[25-31] Among them, semiconducting single-walled carbon nanotube (sc-SWCNT) is a promising candidate for high-performance flexible printed electronics due to its high carrier mobility, excellent chemical stability, mechanical stability, and compatibility with solution-based printing processes. Printed TFTs based on sc-SWCNT have attracted much attention in the past decades and have proven to be fundamental components of [32-34] logic circuits, sensors,[29, 35-38] and displays[39-41]. Various printing methods such as screen printing, inkjet printing, and transfer printing processes have been used to fabricate SWCNT-TFTs on flexible or rigid substrates, but there still needs a breakthrough to achieve industrial production.[42] An important reason is the size and cost limitation of the current mainstream printing process.

Roll-to-roll (R2R) printing technology is promising due to its high-output, large-area, and low-cost advantages. [28, 43, 44] Furthermore, the final packaging of the R2R-printed electronics into product devices is simple and convenient since only cutting and pasting processes are required.[45-48] Although R2R printing has been used to construct SWCNT TFTs on polyethylene terephthalate (PET) rolls for different sensors,[49-52] display active matrices, logic gates and circuits, etc.,[44, 53-55] the reported SWCNT TFTs exhibited poor electrical characteristics (such as low I_{on}/I_{off} ratios, high operation voltage and low mobility) and unstable yield values owing to lack of high-quality sc-SWCNT inks and thin films, and unsuitable printable dielectric materials, which hinders the industrial production of R2R printing.[48, 50, 51, 56, 57]

In this work, we firstly reported an R2R ultra-fast (8 m min^{-1}) printing of large-area (8 cm × 14 cm, theoretically infinite in length, which is limited by the R2R printing machine), high-quality sc-SWCNT thin films on different substrates (PET, Al, and paper) with a fast cure time (<5 s), low cure temperature (<150°C) and without any solvent rinsing after optimizing the sorted sc-SWCNT ink concentrations and printing times. As-prepared sc-SWCNT thin films can be directly used to fabricate top-gated and bottom-gated flexible TFTs and complementary metal oxide semiconductor (CMOS) inverters without any other post-treatment. The fabricated p-type TFT devices showed high carrier mobility (~11.9 cm^2 V^{-1} s^{-1}), high I_{on}/I_{off} ratios (10^5-10^6), small hysteresis (40 mV), and small subthreshold swing (SS) (70-80 mV dec^{-1}) with gate voltage varied from -1 V to 1 V. Furthermore, the constructed flexible CMOS inverters exhibited good properties with rail-to-rail voltage output characteristics (even the operating voltage down to V_{DD} = -0.2 V), voltage gain of 11 at V_{DD} = -0.8 V, and power consumption down to 0.056 nW at V_{DD} = -0.2 V. Compared with other reports about R2R printing SWCNT electronics, our TFT devices and CMOS inverters exhibited more excellent properties. The work demonstrates the potential of R2R printing technology for high-output, large-area, and high-performance carbon-based flexible electronics and circuits.

2. Experimental section

2.1 Materials and Instruments

The carbon nanotubes (P2) were obtained from Carbon Solutions (USA). PCz

polymer (9-(1-octylonoyl)-9H-carbazole-2,7-diyl) was synthesized by ourselves. Silver nanoparticle ink was obtained from Advanced Nano Products Co, DGP 45HTG. The epoxy amine ink used for n-doping and encapsulation was purchased from Xuzhou (China) Zhongyan Technology. The ink contains two compounds: the epoxy resin (128) and the polyamide cross-linking agent (3680). 1-Ethyl-3-methylimidazoliumbis (trifluoro-methylsulfonyl) imide (EMIM-TFSI), poly(4-vinylphenol) (PVP, Sigma Aldrich Inc. M_w = 25 kg mol^{-1}) and poly (melamine-co-formaldehyde) methylated solution (PMF, Sigma Aldrich Inc.M_n = 432 g mol^{-1}, 84 wt% in 1-butanol) were obtained from Sigma-Aldrich. Different types of sc-SWCNT thin films were printed on polyethylene terephthalate (PET), paper and Aluminum substrates using a D&R Lab Gravure Printer G-1100S (Suzhou D&R Instrum Co., Ltd, Suzhou, China). UV-vis-NIR adsorption spectra of sc-SWCNT inks were measured using a LAMBDA 750 UV-vis-NIR spectrometer (Perkin Elmer, Waltham, Massachusetts, USA). The scanning electron microscope (SEM) images of SWCNT films on flexible substrates were obtained using a Hitachi S-4800 instrument (Hitachi Co. Japan). All electrical measurements of SWCNT TFTs and CMOS inverters were carried out using Keithley 2636B or Keithley 4200 analyzer in the air at a V_{DS} of -0.25 V (or 0.25 V) with a sweeping step of -0.01 V (or 0.01 V).

2.2 Preparation of R2R printable inks

To obtain printable sc-SWCNT inks, 6 mg of arc-discharged SWCNT (Carbon Solutions, USA) and 6 mg of PCz polymer (9-(1-octanoyl)-9H-carbazole-2,7-diyl, synthesized in our laboratory) were placed in 10 mL of toluene and then treated at 0°C for 30 min, by probe sonication (Sonics & Materials Inc., Model: VCX 130, 80W). Then the dispersed sc-SWCNT solutions were centrifuged at 40000 g for 2 h to remove metallic carbon nanotubes and insoluble material. To obtain highly concentrated and printable sc-SWCNT inks for R2R gravure printing, the above solutions were enriched by filtration through polytetrafluoroethylene (PTFE) filter membranes and washed by toluene for 3 times to remove residual PCz polymers in SWCNT thin films. As-obtained sc-SWCNTs were redispersed in an appropriate amount of toluene with the aid of sonication in the water bath with a power of 2000 W for 30 min at 0°C. The obtained supernatant can be directly used for R2R gravure

printing without any solvent cleaning.

R2R printed crosslinked poly (4-vinyl phenol) (c-PVP) on flexible substrates acted as the adhesion layer for immobilizing sc-SWCNTs to obtain the proper wettability, which is benefit for consistently transferring sc-SWCNT inks. To obtain the c-PVP solution, 0.223 g PVP was added to 2 mL propylene glycol monomethyl ether (PGMEA) and stirred at 1300 rpm and 90°C for 15 min. After the solution was cooled to room temperature, 70 mg of poly(melamine-co-formaldehyde) (PMF) was added, and the solution was stirred at room temperature (1000 rpm) until the solution was clear and transparent. A cross-linked ionic liquid (IL, [EMIM] [TFSI]) c-PVP (IL-c-PVP) ink consisting of c-PVP and ILs acts as the dielectric inks. The ILs were added into the c-PVP solution and stirred at 1000 rpm for 10 min to obtain the IL-c-PVP inks. PVP, PGMEA, PMF, and [EMIM][TFSI] were purchased from Sigma. The IL-c-PVP inks can be directly used to R2R print the dielectric layers without further purification.

Epoxy amine ink was formulated by mixing the epoxy resin (128) and cross-linking agent polyamide at a mass ratio of 1:1.5 at room temperature and stirring for 30 min. Afterward, the prepared epoxy amine inks were printed into the channels of TFTs for encapsulation and electron doping without further purification.

2.3 Deposition of sc-SWCNT thin films using R2R gravure printing

First, a flatten layer of c-PVP was printed by R2R gravure printing at a speed of 13 m min^{-1} with 75% pressure, then cured at 150°C for 30 min. Then the sc-SWCNT solution was R2R gravure printed at 8 m min^{-1} with 72 % pressure and cured at 90°C for 10 min to evaporate the residual solvent. Conjugated polymer (PCz) sorted sc-SWCNTs can be immobilized on c-PVP-modified flexible substrates effectively due to the hydrophilicity of the c-PVP. The number of R2R gravure printing sc-SWCNT inks was varied to control sc-SWCNT density on flexible substrates (including PET, Al, and paper) by simple rewinding of gravure printing reels. 8 cm × 14 cm thin films (which is limited by our machine) were obtained by R2R gravure printing, and morphologies and electrical properties of R2R printed sc-SWCNT thin films were characterized by SEM and Keithley 2636B or Keithley 4200 analyzer.

2.4 Fabrication and characterization of fully printed SWCNT TFTs and inverters

The fabrication process of fully printed top-gated SWCNT TFTs on PET and paper substrates is illustrated in **Scheme 1**. Prior to the deposition of sc-SWCNT inks, the surface of c-PVP was cleaned by UV-zone for 100 s to enhance the surface adhesion. Then the sc-SWCNT solutions were deposited on the substrate by R2R gravure printing at a speed of 8 m min^{-1} and annealed at 90°C for 3 min (one cycle) without toluene cleaning. The above process was repeated for 5, 10, 12, and 15 times. Subsequently, the sc-SWCNT thin films were patterned by photolithography and oxygen plasma etching to form the desired array of channels. Printed source/drain electrodes were deposited on top of patterned sc-SWCNT thin films by Dimatix Printer (DMP-2831) and annealed in air at 150°C for 30 min. IL-c-PVP inks were R2R gravure printed at the speed of 11 m min^{-1}, followed by pre-annealing at 105°C for 10 min and annealing at 150°C for 90 min to achieve the gate dielectric layer. Finally, the silver gate electrodes were prepared using the same fabrication method of printed source/drain electrodes. Furthermore, the bottom-gated SWCNT TFTs are also constructed using the same process technique with thermal evaporated Al gate electrodes (thickness of 200 nm, to achieve enhancement-mode TFTs) and printed silver gate electrodes. The channel length (L) and width (W) were 110 and 900 μm, respectively. To achieve n-type printed SWCNT TFT devices, epoxy amine inks were selectively printed onto the p-type SWCNT-TFT device channels using a dispenser printing system, and then the samples were baked at 90°C for 5 min. Finally, CMOS inverters were connected by silver conductive lines printed by an inkjet printer. All fabrication process steps were performed under ambient conditions. Electrical characteristics of all TFT devices and CMOS inverters were recorded using Keithley 2636B or Keithley 4200 semiconductor parameter analyzer in a dark environment at room temperature. The field effect mobilities were calculated through the equation

$$\mu = \frac{dI_{ds}}{dV_{gs}} \times \frac{L}{W} \times \frac{1}{V_{DS}C_{i.}}$$
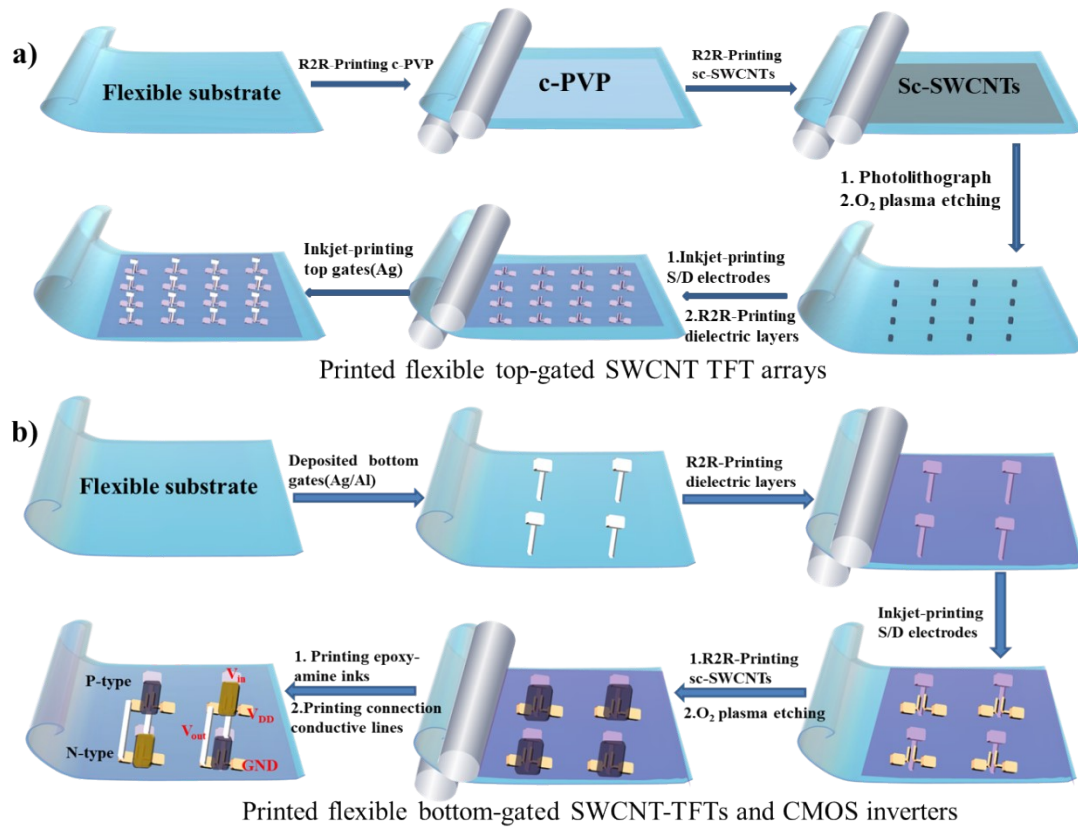
Scheme 1: Schematic diagrams of the fabrication process of R2R gravure printed **a)** top-gated and **b)** bottom-gated SWCNT TFTs and CMOS inverters on flexible substrates including PET, Al, and paper.

3. Results and discussion

Generally, as-prepared polymer-sorted sc-SWCNT inks are unsuitable for R2R gravure printing due to low-concentration sc-SWCNTs and high-concentration polymer in inks. To meet the requirements of R2R gravure printing, PCz-sorted sc-SWCNT inks (the sc-SWCNT absorbance peak height of ~0.3) were filtered by a 0.2 μm filter, and the filtered sc-SWCNT thin films were cleaned by toluene, and then redispersed in toluene to obtain the highly concentrated sc-SWCNT inks (the sc-SWCNT absorbance peak height of 1.8 and 4.5 for ink 2 and 3 as shown in **Figure 1**). It can be seen from **Figure 1b** that the S22 peaks (1000-1200 nm) of the sc-SWCNTs have a sharp peak, and no metal peaks (600-800 nm) are observed. Notably, the peak heights of PCz polymers in sc-SWCNT ink 2 with an sc-SWCNT absorbance peak height of 1.8 is lower than that in as-sorted sc-SWCNTs with an sc-SWCNT absorbance peak height of 0.3 after filtering, indicating that filtering could effectively

remove free PCz polymers in sc-SWCNT inks. The excess polymers in TFT channels could severely hinder the carrier transport in the sc-SWCNT network and reduce the I_{on}/I_{off} ratios of SWCNT TFTs. Later experiments show that the sc-SWCNT inks prepared by this method greatly simplify the fabrication process of TFTs, and excellent electrical properties are obtained without solvent cleaning.
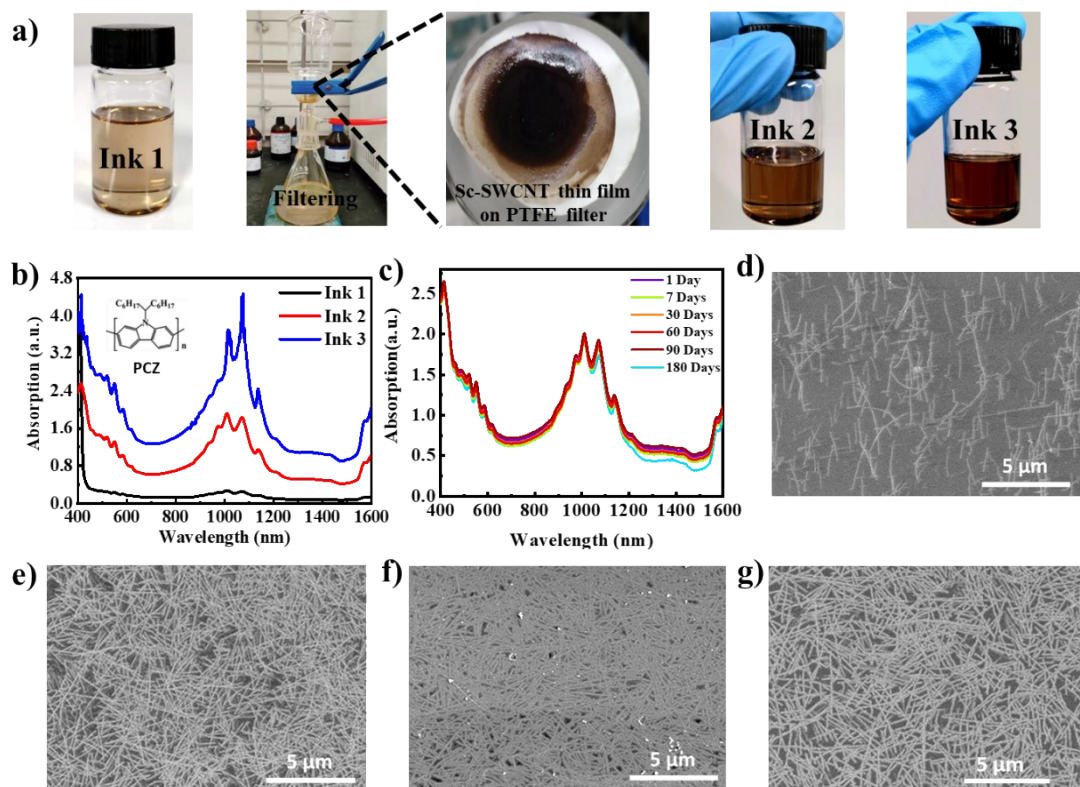

Figure 1: a) Optical images of sorted and concentrated sc-SWCNT inks, and sc-SWCNT thin film on PTFE substrate, **b)** UV-Vis-NIR adsorption spectra of sorted and concentrated sc-SWCNT inks, **c)** UV-Vis-NIR adsorption spectra of ink 2 with the adsorption peak height of 1.8 after storage for 100 days. SEM images of R2R gravure printed SWCNT thin films on PVP-modified PET substrated (the printing speed of 8 m min^{-1}, the printing pressure of 73%, and printing 10 times) using sc-SWCNT inks with the adsorption peak heights of **d)** 0.3, **e)** 1.8, **f)** 3.8, and **g)** 1.8 after storage for 30 days.

The stability of the concentrated inks is also investigated. It can be seen from **Figure 1c** that the highly concentrated sc-SWCNT ink 2 still has excellent dispersion after storage in the air for 180 days. The ink 1-3 with the surface tension of 30-35 mN m^{-1} and a viscosity of 27-30 Cp could provide rheology and adequate ink transferring at a processing speed of 8-12 m min^{-1} during R2R gravure printing without the

addition of binders or surfactants, which can adversely affect the electrical properties of SWCNT TFTs. To evaluate the quality of printing sc-SWCNT thin films, ink 1-3 were R2R gravure printed on c-PVP-modified PET substrates for 10 times and morphologies of sc-SWCNT thin films were characterized by SEM shown in **Figure 1d-g**. It was obvious that high-density sc-SWCNT thin films were observed using the highly concentrated sc-SWCNT ink 2 and 3 after R2R gravure printing for 10 times. However, inks with higher concentrations have more sc-SWCNT bundles and polymer residues (**Figure 1b** and **1f**), which seriously degrade the electrical properties of sc-SWCNT TFTs. **Figure 1f** displays that R2R gravure printed sc-SWCNT thin films are still dense and homogeneous when using ink 2 stored in air for 30 days, demonstrating good long-term stability of the enriched sc-SWCNT ink 2.

To investigate the generalizability of R2R printing of large-area sc-SWCNT thin films on different substrates, we also chose paper substrates and Al foils. It is noted that we attempted to deposit sc-SWCNTs on commercial Al foil (Fabricated by R2R techniques) with the aim of simplifying the fabrication process by using the Al foil directly as the low work function gate electrodes for the fabrication of enhancement-mode P-type SWCNT TFTs. **Figure 2** demonstrates the typical SEM images of sc-SWCNT networks on PET, paper, and Al substrates before and after modification of the c-PVP adhesion layer. It can be seen that few sc-SWCNTs could be observed on substrates without the c-PVP adhesion layer, due to the weak bonding force between sc-SWCNTs and substrates (**Figure 2a-c**). On the other hand, high-density and uniform sc-SWCNT thin films were achieved on c-PVP-modified substrates (**Figure 2d-f**). The density of sc-SWCNTs could reach ~60 tubes μm^{-1} on the c-PVP-modified Al and PET substrates, while the density reduced to ~30 tubes μm^{-1} on the c-PVP-modified paper substrates due to the uneven and porous surface. The insets of **Figure 2** are the water contact angles on corresponding substrates. The water contact angles on PET, Al, and paper substrates without c-PVP adhesion layer were 64.9°, 53.5°, and 81.4°, respectively (inset of **Figure 2a-c**). After being modified by c-PVP thin films, water contact angles on these substrates decreased to 11.6°, 6.8°, and 20.1°, respectively (inset of **Figure 2d-f**). It was attributed to hydroxyl groups on the c-PVP-modified substrates. The SEM and water contact angle results reveal that the c-PVP thin films can act as the adhesion layer to immobilize sc-SWCNTs efficiently, and high-density sc-SWCNT networks were achieved after modification of the c-PVP

adhesion layer. It is noted that some functional groups such as -OH, C-O, -COO- and C=O would be formed on PVP substrates after treatment by oxygen plasma, which are helpful for immobilizing sorted sc-SWCNTs on the c-PVP surfaces of different substrates, probably via strong intermolecular forces (hydrogen bonding/van der Waals/electrostatic force). Therefore, ink 2 and c-PVP thin films are chosen as the R2R printing semiconducting ink and the adhesion layers to immobilize sc-SWCNTs in the following experiments.
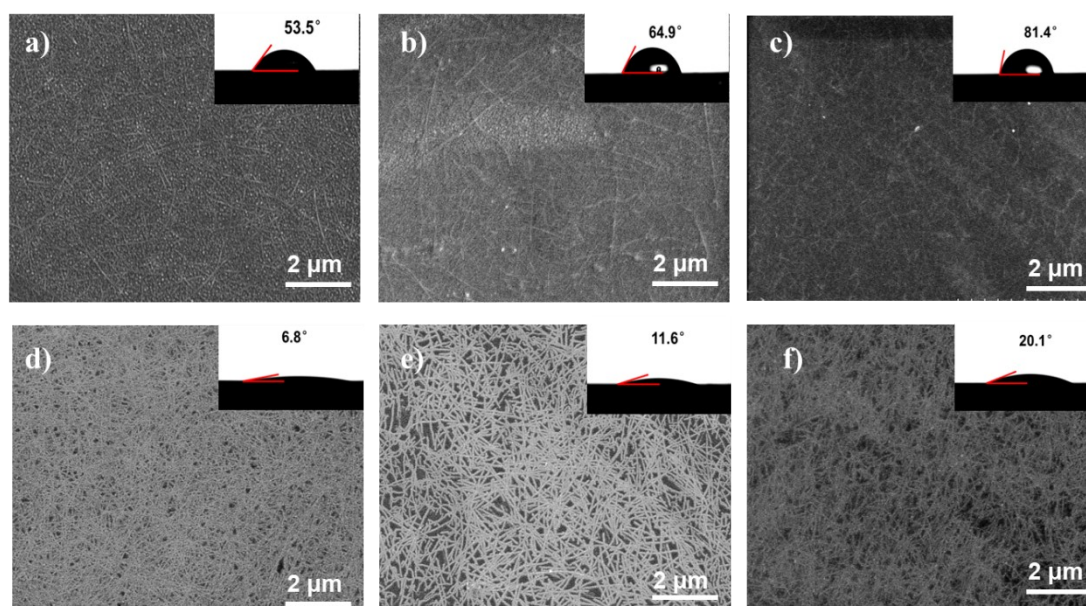

Figure 2: SEM images of sc-SWCNT films on **a)** Al, **b)** PET, and **c)** Paper substrates without c-PVP modification layer, and **d)** Al, **e)** PET and **f)** Paper substrates with c-PVP modification after R2R printing 10 times. The insets are water contact angles of Al, PET, and paper substrates before and after modification of c-PVP thin films by R2R gravure printing.

To investigate the feasibility of R2R gravure printing in fabricating large-area devices, sc-SWCNT thin film deposition on an 8 cm × 14 cm PET substrate was explored. Firstly, the c-PVP adhesion layer was deposited on flexible substrates by R2R gravure printing at a speed of 11 m min⁻¹, and then ink 2 was R2R gravure printed on c-PVP-modified flexible substrates for 10 times with a printing speed of 8 m min⁻¹. As shown in **Figure 3**, dense and uniform sc-SWCNT networks can be obtained in different areas of 8 cm × 14 cm on the PET substrate after R2R gravure printing sc-SWCNT inks for 10 times with a single printing time of 0.1 ms. The results indicated that R2R gravure printing high-purity sc-SWCNT on flexible

substrates is scalable and has the potential for future applications in large-area flexible electronic devices.
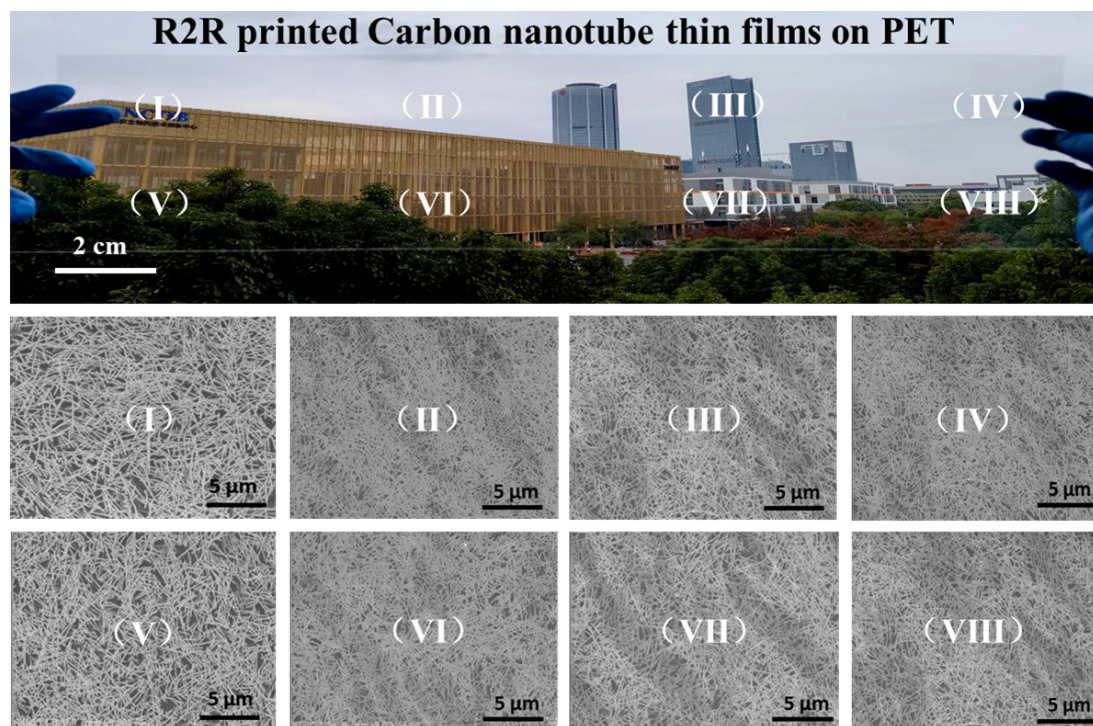

Figure 3: SEM images of sc-SWCNT networks in different areas of 8 cm ×14 cm sc-SWCNT thin films on a PET substrate.

To obtain high-quality R2R printing sc-SWCNT thin films for high-performance TFT devices, 5, 10, 12, and 15 active layers on c-PVP-modified PET substrates were R2R printed with ink 2, and the top-gated printed SWCNT TFTs were then constructed, and electrical properties were evaluated. **Figure 4a-c** and **Figure 3** display the sparse carbon nanotube networks for printing 5, 10, 12, and 15 times. Obviously, the density of sc-SWCNT thin films increases with increasing printing times. At the same time, more carbon nanotube bundles and polymers in sc-SWCNT thin films were observed shown in **Figure 4b** and **4c**, which can block carrier transports in carbon nanotube networks. The corresponding electrical characteristics of sc-SWCNT TFTs are displayed in **Figure 4d-f**. It can be seen from **Figure 4d** that the on-currents of printed SWCNT TFTs increased with increasing sc-SWCNT printing times due to increasing sc-SWCNT density in the TFT channels, and the I_{on}/I_{off} ratios, μ_{FE}, hysteresis, and SS decrease when the printing times are more than 10 times. As shown in **Figure 4d-f**, the optimum I_{on}/I_{off} ratio (10^6), μ_{FE} (11.9 cm^{2}V^{-1}s^{-1}), hysteresis ($\triangle V_{HYST}$ ~30 mV) and SS (70 mV dec^{-1}) of printed SWCNT TFTs were

obtained when R2R printing 10 times. However, Further increasing printing sc-SWCNT ink times could decrease the electrical properties of printed SWCNT TFTs, which is ascribed to that the carrier transport is affected by the formation of sc-SWCNT bundles and the increased polymers in SWCNT thin films.
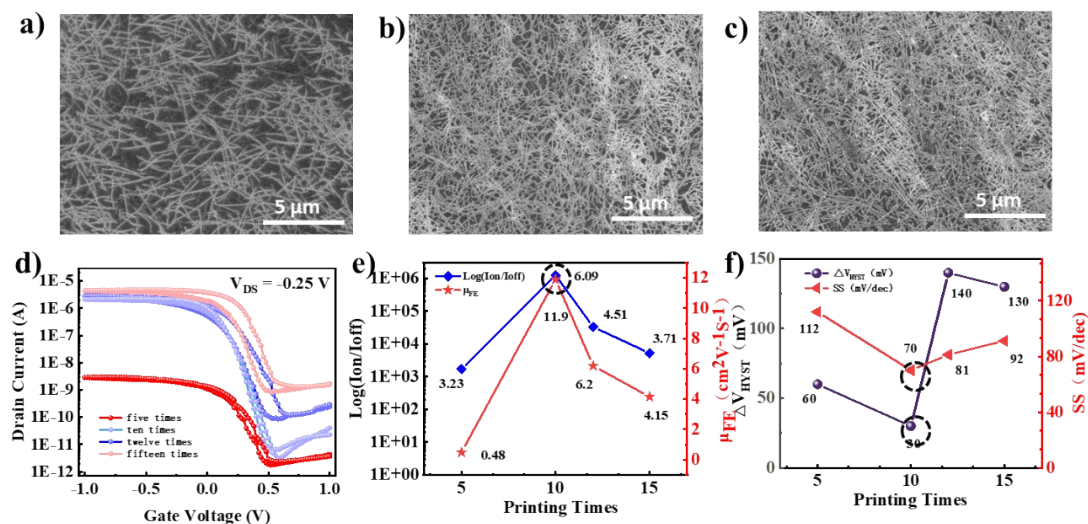

Figure 4: SEM images of R2R gravure printed SWCNT thin films with different printing times using sc-SWCNT inks with the adsorption peak height of 1.8. **a)** 5 times, **b)** 12 times, and **c)** 15 times, **d)** the corresponding transfer curves, **e)** calculated I_{on}/I_{off} and μ_{FE}, and **f)** SS and $\triangle V_{HYST}$ of fully printed SWCNT-TFTs.

Figure 5a and **5b** illustrate the fully printed top-gated SWCNT TFT arrays and SEM images of sc-SWCNT channels on PET and paper substrates, respectively. The transfer characteristics of as-prepared SWCNT-TFTs on PET and paper substrates are illustrated in **Figure 5c-h**. All devices exhibited typical p-type behavior due to the adsorption of oxygen and moisture from the ambient environment at the channel area, and excellent mechanical flexibility after bending 10000 or 5000 times with a curvature radius of 5 mm. It is noted that printed SWCNT TFTs on PET substrates show more excellent electrical properties (higher I_{on}/I_{off} ratios, mobility, and smaller SS) than those on paper substrates. It can be observed from the optical image in **Figure 5b** that the surface of the paper substrate is very rough and porous, resulting in the unclean etching during the patterning of sc-SWCNT thin films by oxygen plasma and higher off currents than those on other substrates. **Table 1** summarizes the electrical parameters extracted from the transfer curves of fully printed SWCNT TFTs on the PET and paper substrates (12 devices), exhibiting satisfied electrical properties. Printed SWCNT TFTs on PET substrates had low threshold voltage, high I_{on}/I_{off} ratio

($\geq 10^6$), small SS (70-80 mV dec^{-1}), and small hysteresis ($\triangle V_{HYST}$ = 40±5 mV), as well as high carrier mobility (μ_{FE} = 9.79±0.5 cm^2 V^{-1} s^{-1}) at low gate voltages (±1 V). Although the rough and porous structure of paper substrates led to decreased I_{on}/I_{off} ratios of TFTs, SWCNT TFTs on paper substrates still have small SS (~78 mV dec^{-1}) and high μ_{FE} (~4.53 cm^2 V^{-1} s^{-1}).
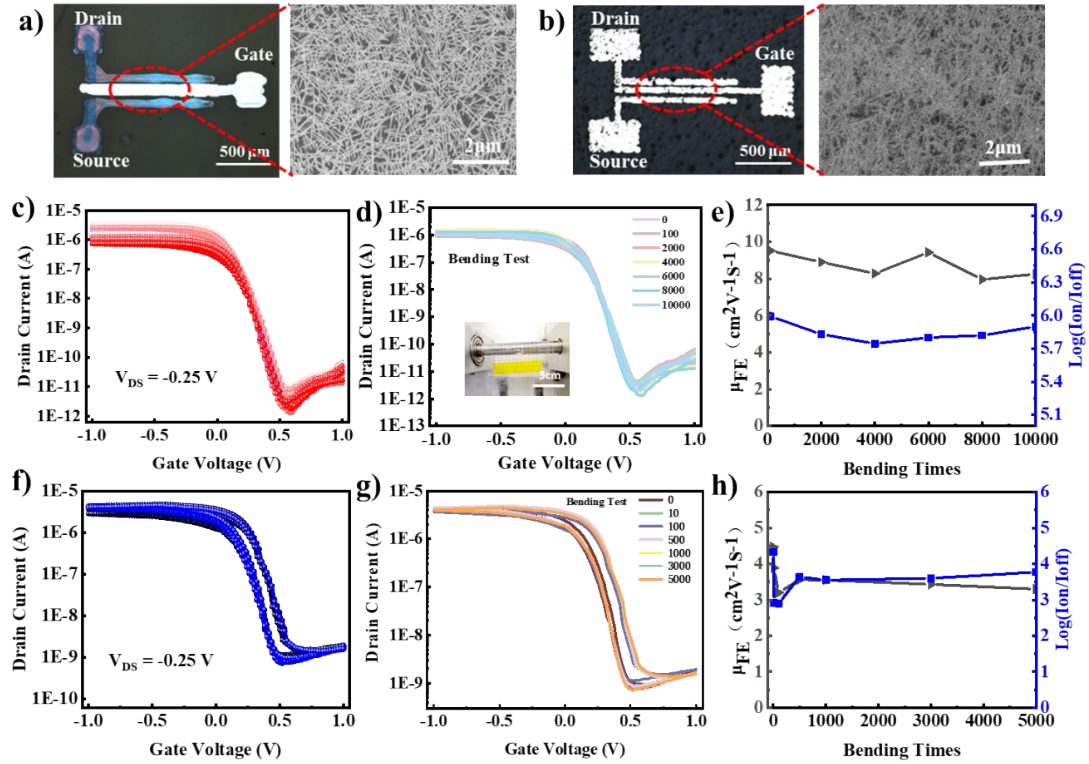

Figure 5: Optical images of fully printed SWCNT TFTs and SEM images of sc-SWCNT thin films in device channels on **a)** PET and **b)** paper substrate. **c)** Transfer curves of fully printed SWCNT TFTs on PET substrate, and **d)** and **e)** mechanical flexibility properties after bending 10000 times with a curvature radius of 5 mm (V_{DS}= -0.25 V). **f)** Transfer curves of fully printed SWCNT TFTs on paper substrates, and **g)** and **h)** mechanical flexibility properties after bending 5000 times with a curvature radius of 5 mm (V_{DS} = -0.25 V). The inset in **Figure 5d** is the photograph of the flexible devices wrapped on a cylinder with a curvature radius of 5 mm.

The mechanical bending tests were performed to evaluate the mechanical stability of fully printed top-gated SWCNT TFTs on PET and paper substrates. **Figure 5d** shows the measured transfer curves of the fully printed SWCNT TFTs on PET substrate after 10000 bending cycles. No significant electrical properties (μ_{FE} and I_{on}/I_{off}) degradation was observed after 10000 bending cycles. **Figure 5e** displays

the bending time as a function of extracted μ_{FE} and I_{on}/I_{off} ratios; no significant electrical properties degradation was observed after 10000 bending cycles. The outstanding mechanical flexibility and reliability of fully printed SWCNT TFTs on PET substrates can be attributed to the mechanical compatibility of IL-c-PVP solid-state electrolytes and the mechanical flexibility of sc-SWCNTs, as well as the excellent bending resistance of the PET substrate. **Figure 5f-h** demonstrate the measured transfer curves of the fully printed SWCNT TFTs on the paper substrate after 5000 bending cycles. No significant changes were observed after bending 5000 cycles. However, the I_{on} decreased, and the transfer curves became unsmooth when further increasing the number of bending cycles.

Table 1 The average electrical properties and standard deviations of printed SWCNT TFTs (12 devices) extracted from the transfer characteristics (**Figure 5c** and **5f**) in the linear regions.

Substrate	SS (mV dec^{-1})	ΔV_{HYST}(mV)	I_{on}/I_{off}	μ_{FE}(cm^2 V^{-1} s^{-1})
PET	72±5	40±5	~10^6	9.79±0.5
Paper	**78±6**	**140±10**	**10^3-10^4**	**4.53±0.8**

To facilitate the development of CMOS circuits, we developed the R2R bottom-gated SWCNT TFTs with a similar manufacturing process (**Scheme 1b)**. It can be known that enhancement-mode TFTs can be obtained by reducing the work function of the gate electrodes.[38] The enhancement-mode and depletion-mode bottom-gate/top contact TFTs were obtained when using the Al gate electrodes with low work function native aluminum oxide (As a result, the holes in the TFT channel were depleted, and a negative threshold voltage shift was observed.) and the silver gate electrodes are shown in **Figure 6a-c**. It can be seen from **Figure 5c** and **Figure 6c** that both of I_{on}/I_{off} ratios and mobility of bottom-gated SWCNT TFTs are similar to those of top-gated SWCNT TFTs. N-type SWCNT TFTs were achieved by covering the epoxy-amine inks on the channel of p-type TFTs (**Figure 6d)**. The prepared p-type and n-type SWCNT TFTs exhibited almost symmetric electrical properties in the ambient environment (**Figure 6e)**. It is worth noting that the I_{on} of the SWCNT-TFTs during the polarity transition remained no obvious changesunchanged. This is due to the solidified state of the polarization transfer solution and low air and water oxygen
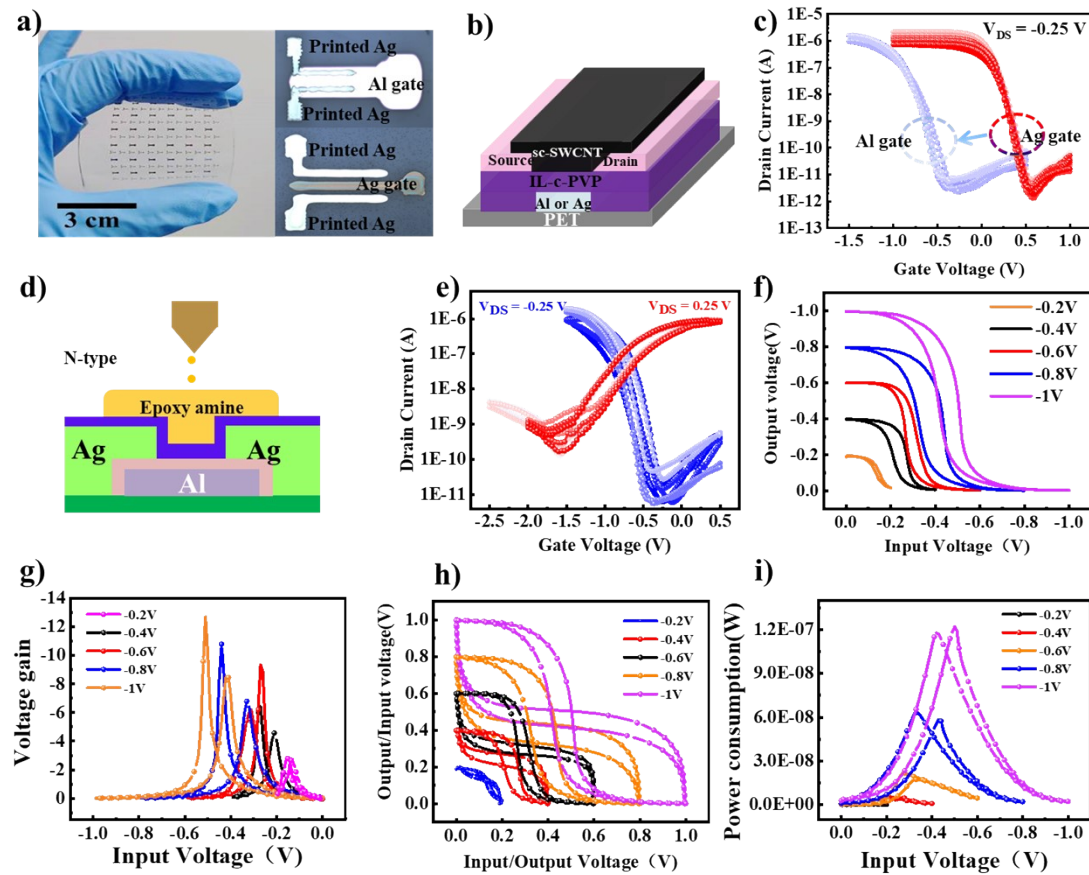
density in the environment.

Figure 6: a) Optical and magnified optical images of printed SWCNT TFTs, **b)** the structure of a printed bottom-gated printed SWCNT TFT, **c)** typical transfer characteristics of fully printed Ag-gate SWCNT TFTs and Al-gate SWCNT TFTs on PET substrates. **d)** The structure of a printed n-type bottom-gated printed SWCNT TFT, **e)** transfer characteristics of p-type and n-type SWCNT TFTs with V_{DS} = -0.25 V and 0.25 V, respectively. **f)** Input/Output voltage curves, **g)** voltage gains, **h)** noise tolerance, **i)** power consumption of the printed CMOS inverter with input voltages from -0.2 V to -1 V.

To demonstrate the potential of R2R gravure printed high-speed, large-area, low-cost SWCNT TFTs for the realization of ultra-low voltage CMOS circuits in the fields of electronic skin, flexible neuromorphic devices, intelligent wearable devices and systems, printed SWCNT CMOS inverters were constructed by connecting two unipolar n-type and p-type TFTs, as shown in **Figure 6e**. The performance of p-type and n-type SWCNT TFTs used in the CMOS inverter are displayed in **Scheme 1b**. The voltage gain, power dissipation, and noise margins were extracted from the static

inverter characteristics to evaluate whether the printed CMOS inverters are suitable for integrating complicated and high-performance logic circuits with low power consumption. **Figure 6f** indicates that the printed CMOS inverters exhibited full rail-to-rail voltage operation with V_{DD} down to -0.2 V. As shown in **Figure 6g**, the voltage gains (dV_{out}/dV_{in}) of the printed CMOS inverters were 10. 8 and 12.8 at V_{DD} = -0.8 V and V_{DD} = -1 V, respectively. The noise margins of printed CMOS inverter with input voltages from -0.4 V to -1 V are 38%, 50%, 56%, 60% of 1/2 V_{DD} (**Figure 6h**). Another important feature of portable devices is the power dissipation ($P_W = I_{DD} \times V_{DD}$), as demonstrated in **Figure 6i**. The power dissipation of the printed CMOS inverters was 0.51 nW at V_{DD} = -0.4 V, and the lowest power consumption 0.056 nW was achieved at V_{DD} = -0.2 V. It is noted that as-prepared enhancement-mode p-type and n-type SWCNT TFTs exhibited almost symmetric electrical properties with low off-currents and low leakage currents and the printed CMOS inverters exhibited full rail-to-rail voltage operation. Such a low power consumption could be attributed to well-matched CMOS TFTs with relatively low off-currents and low leakage currents ($\sim 10^{-10}$ A).

4. Conclusion

In summary, we developed a universal approach to construct large area and high-quality sc-SWCNT thin films on flexible substrates (PET, paper, and Al substrates) by R2R gravure printing using highly concentrated sc-SWCNT inks and c-PVP films as the adhesion layer. The fully printed flexible SWCNT TFTs based on R2R gravure printed sc-SWCNT thin films exhibited excellent mechanical flexibility and good electrical properties with a high I_{on}/I_{off} ratio ($\sim 10^6$), small SS (~ 70 mV dec^{-1}), small hysteresis, and high carrier mobility (~ 11.9 cm^2 V^{-1} s^{-1}) at gate voltage between -1 V and 1 V. Moreover, the fully printed inverters exhibited rail-to-rail output swings with voltage gain up to 12.8 at V_{DD} = -1 V and the power consumption down to 0.056 nW at V_{DD} = -0.2 V. Overall. This work overcame the performance, cost, size, and efficiency limitations of conventional materials and printing methods, which could promote the development of fully printed low-cost, large-area, high-output, and flexible carbon-based electronics. To meet the demands of R2R gravure printing, we

will focus on developing the directly patternable sc-SWCNT inks using high viscosity, high polar and low toxicity solvents, and optimizing the R2R gravure printing process.

Author information

Corresponding Authors

*Email: jwzhao2011@sinano.ac.cn (J.W. Zhao.);

yxfang2021@sinano.ac.cn (Y.X. Fang).

ORCID

Jianwen Zhao: 0000-0002-5548-5469

Yuxiao Fang: 0000-0002-0845-1936

Notes

The authors declare no competing financial interest.

Acknowledgment

References

1   M. Saadi, A. Maguire, N. T. Pottackal, M. S. H. Thakur, M. M. Ikram, A. J. Hart, P. M. Ajayan and M. M. Rahman, *Adv. Mater.,* 2022, **34**, 2108855.

2   F. Liao, J. Deng, X. Chen, Y. Wang, X. Zhang, J. Liu, H. Zhu, L. Chen, Q. Sun, W. Hu, J. Wang, J. Zhou, P. Zhou, D. W. Zhang, J. Wan and W. Bao, *Small,* 2020, **16**, 1904369.

3   A. Liu, H. Zhu, S. Bai, Y. Reo, T. Zou, M.-G. Kim and Y.-Y. Noh, *Nature Electronics,* 2022, **5**, 78-83.

4   J.-L. Meng, T.-Y. Wang, L. Chen, Q.-Q. Sun, H. Zhu, L. Ji, S.-J. Ding, W.-Z. Bao, P. Zhou and D. W. Zhang, *Nano Energy,* 2021, **83**, 105815.

5   A. Corletto and J. G. Shapter, *ACS Appl. Nano Mater.,* 2020, **3**, 8148-8160.

6   W. Gao, S. Emaminejad, H. Y. Y. Nyein, S. Challa, K. Chen, A. Peck, H. M. Fahad, H. Ota, H.

Shiraki, D. Kiriya, D. H. Lien, G. A. Brooks, R. W. Davis and A. Javey, *Nature,* 2016, **529**, 509-514.

7   A. A. Marunchenko, M. A. Baranov, E. V. Ushakova, D. R. Ryabov, A. P. Pushkarev, D. S. Gets, A. G. Nasibulin and S. V. Makarov, *Adv. Funct. Mater.,* 2021, **32**, 2109834.

8   K. Schnittker, M. Tursunniyaz and J. B. Andrews, *J. Inf. Disp.,* 2021, **22**, 193-209.

9   H. Y. Y. Nyein, M. Bariya, B. Tran, C. H. Ahn, B. J. Brown, W. Ji, N. Davis and A. Javey,   *Nat. Commun.,* 2021, **12**, 1823.

10   J. Pang, A. Bachmatiuk, F. Yang, H. Liu, W. Zhou, M. H. Rummeli and G. Cuniberti, *Nano-Micro Lett.,* 2021, **13**, 191.

11   Y. Tchoe, J. Lee, R. Liu, A. M. Bourhis, R. Vatsyayan, K. J. Tonsfeldt and S. A. Dayeh, *Appl. Phys. Rev.,* 2021, **8**, 041317.

12   S. Qiu, K. Wu, B. Gao, L. Li, H. Jin and Q. Li, *Adv. Mater.,* 2019, **31**, 1800750.

13   T. Gao, J. Deng, X. Li, Y. Ren, W. Gu, M. Robin and J. Zhao, *J. Mater. Chem. C.,* 2021, **9**, 6852-6862.

14   E. Li, C. Gao, R. Yu, X. Wang, L. He, Y. Hu, H. Chen, H. Chen and T. Guo, *Nat. Commun.,* 2022, **13**, 2898.

15   P. Schulz, A. M. Dowgiallo, M. Yang, K. Zhu, J. L. Blackburn and J. J. Berry, *J. Phys. Chem. Lett.,* 2016, **7**, 418-25.

16   R. Shiwaku, H. Matsui, K. Hayasaka, Y. Takeda, T. Fukuda, D. Kumaki and S. Tokito, *Adv. Electron. Mater.,* 2017, **3**, 1600557.

17   C. Du, Y. Ren, Z. Qu, L. Gao, Y. Zhai, S. T. Han and Y. Zhou, *Nanoscale,* 2021, **13**, 7498-7522.

18   D. Fong, W. J. Bodnaryk, N. A. Rice, S. Saem, J. M. Moran-Mirabal and A. Adronov, *Chem. Eur.,* 2016, **22**, 14560-6.

19   D. Heimfarth, M. Balci Leinen, P. Klein, S. Allard, U. Scherf and J. Zaumseil, *ACS Appl. Mater. Interfaces,* 2022, **14**, 8209-8217.

20   D. Kiriya, K. Chen, H. Ota, Y. Lin, P. Zhao, Z. Yu, T. J. Ha and A. Javey, *Am. Chem. Soc.,* 2014, **136**, 11188-94.

21   J. Lefebvre, J. Ding, Z. Li, P. Finnie, G. Lopinski and P. R. L. Malenfant, *Acc Chem Res,* 2017, **50**, 2479-2486.

22   F. Li, H. Wang, D. Kufer, L. Liang, W. Yu, E. Alarousu, C. Ma, Y. Li, Z. Liu, C. Liu, N. Wei, F. Wang, L. Chen, O. F. Mohammed, A. Fratalocchi, X. Liu, G. Konstantatos and T. Wu, *Adv. Mater.,* 2017, **29**, 1602432.

23   M. Si, Z. Lin, Z. Chen, X. Sun, H. Wang and P. D. Ye, *Nat. Electron.,* 2022, **5**, 164-170.

24   X. Wang, M. Zhu, X. Li, Z. Qin, G. Lu, J. Zhao and Z. Zhang, *Adv. Mater.,* 2022, **34**, 2204066.

25   M. Li, Z. Xiong, S. Shao, L. Shao, S.-T. Han, H. Wang and J. Zhao, *Carbon,* 2021, **176**, 592-601.

26   X. Li, Y. Ren, X. Wang, S. Shao, H. Li, L. Wu, X. Liu and J. Zhao, *Adv. Electron. Mater.,* 2021, **7**, 2001025.

27   X. Li, X. Wang, J. Deng, M. Li, S. Shao and J. Zhao, *Carbon,* 2022, **191**, 267-276.

28   Z. Li, J. Ding, F. Lapointe and P. R. L. Malenfant, *J. Mater. Sci.: Mater. Electron.,* 2021, **32**, 23923-23934.

29   Y. Ren, M. Li, X. Li, Y. Geng, X. Wang and J. Zhao, *J. Mater. Chem. C.,* 2021, **9**, 2133-2144.

30   M. Song, Y. Sun, Z. Liu, B. Wei, H. Wang, J. Yuan, Y. Chen, X. Yang and D. Xie, *Carbon,* 2021, **184**, 295-302.

31   W. Xu, M. Li, M. Tange, L. Li, J. Hou, J. Ye, L. Wei, Y. Chen and J. Zhao, *Nano Res.,* 2022, **15**,

5517-5526.

32   J. Deng, X. Li, M. Li, X. Wang, S. Shao, J. Li, Y. Fang and J. Zhao, *Nanoscale,* 2022, **14**, 4679-4689.

33   J. K. Han, J. Oh, G. J. Yun, D. Yoo, M. S. Kim, J. M. Yu, S. Y. Choi and Y. K. Choi, *Sci. Adv.,* 2021, **7**, 8836.

34   S. Schneider, J. M. Gotthardt, L. Steuer, S. Leingang, H.-J. Himmel and J. Zaumseil, *J. Mater. Chem. C.,* 2021, **9**, 7485-7493.

35   J. A. Cardenas, J. B. Andrews, S. G. Noyce and A. D. Franklin, *Nano Futures,* 2020, **4**.

36   Y. Geng, Y. Ren, X. Wang, J. Li, L. Portilla, Y. Fang and J. Zhao, *Sens. Actuators, B,* 2022, **360**, 131633.

37   T. Pandhi, A. Chandnani, H. Subbaraman and D. Estrada, *Sensors,* 2020, **20**, 5642.

38   X. Wang, M. Wei, X. Li, S. Shao, Y. Ren, W. Xu, M. Li, W. Liu, X. Liu and J. Zhao, *ACS Appl. Mater. Interfaces,* 2020, **12**, 51797-51807.

39   M. Ben Basat and N. Lachman, *Nanomaterials,* 2021, **11**, 2618.

40   F. Cao and L. Li, *Adv. Funct. Mater.,* 2020, **31**, 2008275.

41   S. Lu and A. D. Franklin, *Nanoscale,* 2020, **12**, 23371-23390.

42   L. Wu, Y. Yu and J. Zhi, *RSC Advances,* 2015, **5**, 10159-10164.

43   Y. Y. Kim, T. Y. Yang, R. Suhonen, A. Kemppainen, K. Hwang, N. J. Jeon and J. Seo, *Nat. Commun.,* 2020, **11**, 5146.

44   J. Sun, H. Park, Y. Jung, G. Rajbhandari, B. B. Maskey, A. Sapkota, Y. Azuma, Y. Majima and G. Cho, *ACS Omega,* 2017, **2**, 5766-5774.

45   T. A. M, H. Moon, G. Cho and J. Lee, *Jpn. J. Appl. Phys.,* 2022, **61**, SE0802.

46   Q. Cao, *Nano Res.,* 2021, **14**, 3051-3069.

47   M. Choi, B. Jang, W. Lee, S. Lee, T. W. Kim, H.-J. Lee, J.-H. Kim and J.-H. Ahn, *Adv. Funct. Mater.,* 2017, **27**, 1606005.

48   J. Noh, K. Jung, J. Kim, S. Kim, S. Cho and G. Cho, *IEEE Electron Device Lett.,* 2012, **33**, 1574-1576.

49   Y. Jung, J. Park, J. Sun, H. Park, S. Parajuli, S. Shrestha, K. Shrestha, Y. Majima and G. Cho, *Adv. Mater. Technol.,* 2021, **7**, 2101243.

50   W. Lee, H. Koo, J. Sun, J. Noh, K. S. Kwon, C. Yeom, Y. Choi, K. Chen, A. Javey and G. Cho, *Sci. Rep.,* 2015, **5**, 17707.

51   J. Sun, A. Sapkota, H. Park, P. Wesley, Y. Jung, B. B. Maskey, Y. Kim, Y. Majima, J. Ding, J. Ouyang, C. Guo, J. Lefebvre, Z. Li, P. R. L. Malenfant, A. Javey and G. Cho, *Adv. Electron. Mater.,* 2020, **6**, 1901431.

52   Z. Zhang, B. Wang, J. Qiu and S. Wang, *Manufacturing Letters,* 2019, **21**, 28-34.

53   C. M. Homenick, R. James, G. P. Lopinski, J. Dunford, J. Sun, H. Park, Y. Jung, G. Cho and P. R. L. Malenfant, *ACS Appl. Mater. Interfaces,* 2016, **8**, 27900-27910.

54   Q. Zhang, Y. Ren, Z. Wang, X. Chen, L. Portilla, L. Sun, D. Zhang and J. Zhao, *Flexible Printed Electron.,* 2022, **7**, 015007.

55   J. Sun, K. Shrestha, H. Park, P. Yadav, S. Parajuli, S. Lee, S. Shrestha, G. R. Koirala, Y. Kim, K. A. Marotrao, B. B. Maskey, O. C. Olaoluwa, J. Park, H. Jang, N. Lim, Y. Jung and G. Cho, *Adv. Mater. Technol.,* 2019, **5**, 1900935.

56   H. Koo, W. Lee, Y. Choi, J. Sun, J. Bak, J. Noh, V. Subramanian, Y. Azuma, Y. Majima and G. Cho, *Sci. Rep.,* 2015, **5**, 14459.

57   J. Noh, J. Minhun, J. Kyunghwan, L. Gwangyong, K. Joonseok, L. Soyeon, K. Daae, C. Youngchul, K. Yoonjin, V. Subramanian and C. Gyoujin, *IEEE Electron Device Lett.,* 2011, **32**, 638-640.